Eur. Phys. J. B **16**, 549–561 (2000)

THE EUROPEAN PHYSICAL JOURNAL B

EDP Sciences

A statistical estimator of turbulence intermittency in physical and numerical experiments

Y. Malécot[1,a], C. Auriault[1], H. Kahalerras[1], Y. Gagne[1], O. Chanal[2], B. Chabaud[2], and B. Castaing[2]

[1] LEGI/IMG - CNRS, BP 53X, 38041 Grenoble Cedex 9, France
[2] CRTBT/CNRS/UJF et Institut Universitaire de France, BP 166X, 38042 Grenoble Cedex, France

Received 7 January 2000 and Received in final form 17 March 2000

Abstract. The velocity increments statistic in various turbulent flows is analysed through the hypothesis that different scales are linked by a multiplicative process, of which multiplier is infinitely divisible. This generalisation of the Kolmogorov-Obukhov theory is compatible with the finite Reynolds number value of real flows, thus ensuring safe extrapolation to the infinite Reynolds limit. It exhibits a β estimator universally depending on the Reynolds number of the flow, with the same law either for Direct Numerical Simulations or experiments, both for transverse and longitudinal increments. As an application of this result, the inverse dependence $R_\lambda = f(\beta)$ is used to define an unbiased R_λ value for a Large Eddy Simulation from the resolved scales velocity statistics. However, the exact shape of the multiplicative process, though independent of the Reynolds number for a given experimental setup, is found to depend significantly on this setup and on the nature of the increment, longitudinal or transverse. The asymmetry of longitudinal velocity increments probability density functions exhibits similarly a dependence with the experimental setup, but also systematically depends on the Reynolds number.

PACS. 47.27.-i Turbulent flows, convection, and heat transfer – 47.27.Gs Isotropic turbulence; homogeneous turbulence – 47.27.Jv High-Reynolds-number turbulence

1 Introduction

In order to improve the modelling of turbulent flows, a better knowledge of the small scale intermittency is still needed. The main feature of the intermittency is that the shape of the probability density functions (here after pdf) of the velocity increments $\delta u(r)$ at a given scale r are not the same at each scale, as assumed in [1]. It roughly evolves from a Gaussian shape near the integral scale L to a stretched exponential shape near the Kolmogorov scale η (see Fig. 1). Several intermittency models have been proposed to take into account this effect (see for instance [2–4]). All these models assume a total scale invariance for the velocity field. Actually, as revealed by the behaviour of the velocity structure function there is no scale invariance in the finite Reynolds number flows [5]. However, the velocity field has some kind of self similarity properties [6,7] that the Extented Self Similarity (hereafter ESS) technique has revealed [8]. A few models have recently been proposed which predict that all the scales of the flow dynamically "feel" the viscosity, whatever the Reynolds number can be (the variational approach [9], or the multifractal intermediate dissipation range [10]).

In this context, it is of prime importance to distinguish between models and analysis. The analysis, by the measured quantities and the way they are defined, not only allows to verify the predictions of the various models, but also must check, as far as possible, the underlying hypothesis of these models.

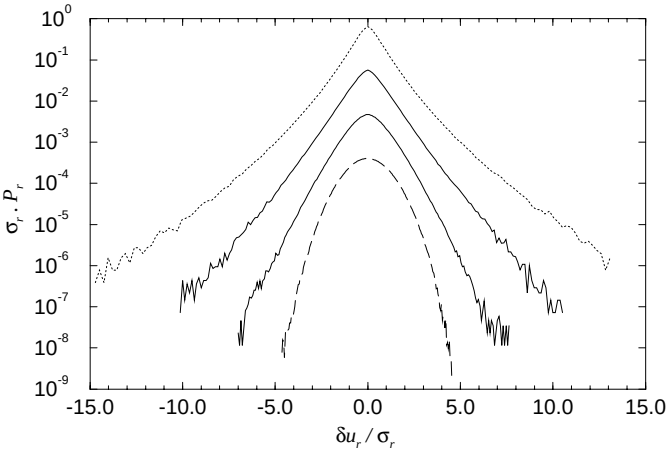

Fig. 1. Normalised pdfs of transverse velocity increments in a turbulent air jet at $R_\lambda = 695$; $r \sim \eta$ (dotted line); $r \sim L$ shifted of three decades (long dashed line); intermediate scales (solid line).

[a] e-mail: yann.malecot@ujf-grenoble.fr

Therefore, a technic of analysis which does not *a priori* assume neither scale invariance nor ESS is necessary. This is the case for the analysis introduced by Castaing *et al.* [11] which has later yielded to the cumulant analysis (*cf.* [12–16] for the generalized wavelet version). This is also the case of the recent Markovian approach of Friedrich and Peinke [17].

In a previous paper, [15], the cumulant analysis, used in this paper and explained in Section 2, has revealed a dependence of an intermittency statistical estimator (defined as the intermittency exponent β) on the Reynolds number of the flow, only for longitudinal velocity increments obtained from physical experiments. In this experimental paper, this data analysis is generalized both to transverse velocity increments and to data obtained by Jiménez *et al.* [18], from direct numerical simulations (DNS).

The purpose is not, *a priori*, to verify the theoretical predictions of the variational model [11], but to bring in evidence some measurable parameters which characterise scale intermittency and to discuss their physical significance and their possible universality in relation to the Reynolds number and the flow type.

Section 3 describes the evolution of the intermittency along the scales for several types of flows obtained from physical and numerical experimental data. Section 4 gives the behaviour of the main characteristic parameters of the intermittency *versus* the Reynolds number. The asymmetry of the longitudinal pdfs is discussed and analysed in Section 5. In Section 6, we apply this analysis to estimate the Taylor Reynolds number (hereafter, noted R_λ) of a flow calculated with a LES.

2 Background of the analysis

2.1 Basic hypotheses

The method introduced in [11] is based on two main hypotheses.

The first hypothesis is to assume that the velocity increments pdf at a scale r, noted $P_r(\delta u)$, can be expressed as a superposition of rescaled velocity increments pdf at a scale l, for any r and l, with l larger than r. That is to say, it is possible to define a positive independent multiplier random variable α_{rl} such as:

$$\delta u(r) \,=\, \alpha_{rl}\ \delta u(l) \quad \forall\ r,\ l \ \text{ with } \ r \leq l.$$

This can also be written in terms of pdf:

$$P_r(\delta u) = \int G_{rl}(\ln \alpha)\, \frac{1}{\alpha}\, P_l\!\left(\frac{\delta u}{\alpha}\right) \mathrm{d}\ln \alpha \qquad (1)$$

where G_{rl} is the pdf of the logarithm of the α_{rl} multiplier.

Then, this analysis only considers the symmetrical part of the velocity increments. This permits to take the logarithm of δu and to transform (1) in a convolution product:

$$(1) \ \Rightarrow \ \bar{P}_r(\ln|\delta u|) = \int G_{rl}(\ln\alpha)\bar{P}_l(\ln|\delta u| - \ln\alpha)\,\mathrm{d}\ln\alpha$$
$$\Leftrightarrow \quad \bar{P}_r = G_{rl} \otimes \bar{P}_l \qquad (2)$$

where $\bar{P}_r$ is the pdf of $\ln(|\delta u(r)|)$.

Before going farther let us note that this point of view is closely related to the recent work of Friedrich and Peinke [17] where the evolution of P_r along the scale is given by a Fokker Planck equation. The connection between the two approaches is discussed in [14] and in the appendix.

Since the previous relation is true whatever the scales r and l are, we have:

$$G_{rl} = G_{rr_{n-1}} \otimes ... \otimes G_{r_1 l} \ \text{ with } \ r \leq r_{n-1} \leq ... \leq r_1 \leq l.$$

The second hypothesis, which is the strongest one, assumes that the r_i can be chosen so that all the $G_{r_i r_{i-1}}$ are the same distribution H. In this case, we have:

$$G_{rl} = H^{\otimes n_{rl}} \qquad (3)$$

where n_{rl} is the number of steps to go from l to r in the cascade, with arbitrary steps H.

At infinite R_λ, this assumption is easy to prove because a total scale invariance is ensured [19]. Indeed the pdf G_{rl} can then only depend on the ratio $\frac{r}{l}$ and not independently on r and l. It is then sufficient to take

$$\frac{r_i}{r_{i-1}} = \frac{r_j}{r_{j-1}} = \left(\frac{r}{l}\right)^{\frac{1}{n}}$$

to ensure that, for any i and j,

$$G_{r_i r_{i-1}} = G_{r_j r_{j-1}}.$$

In finite R_λ case, we will see in Section 3.2 that this hypothesis is equivalent to the ESS that has been experimentally verified [20].

2.2 Cumulant expansion of the velocity structure functions

Assuming that the G distribution is defined, the problem now consists in determining it. From an experimental point of view, we can measure the structure functions of the velocity increments, $\langle|\delta u(r)|^p\rangle$, which are also directly linked to the cumulant generating function ψ_{rl} of the G_{rl} distribution [20].

By definition

$$\ln\langle\alpha_{rl}^p\rangle = \ln\frac{\langle|\delta u(r)|^p\rangle}{\langle|\delta u(l)|^p\rangle}$$

and

$$\begin{aligned}\psi_{rl}(p) \ &= \ln\langle\alpha_{rl}^p\rangle \\ &= C_{1rl}p + C_{2rl}\tfrac{p^2}{2} + ... + C_{irl}\tfrac{p^i}{i!} + ...\end{aligned}$$

Experimentally, the first cumulants are estimated with a polynomial fit of $\psi_{rl}(p)$. In Figure 2, we have plotted the four first cumulants calculated from a fifth order fit of the longitudinal increments measured in the air jet ($R_\lambda = 695$). We clearly observe that there is an order of magnitude between each cumulant. Moreover, the signal to noise ratio decreases with the order p, so that

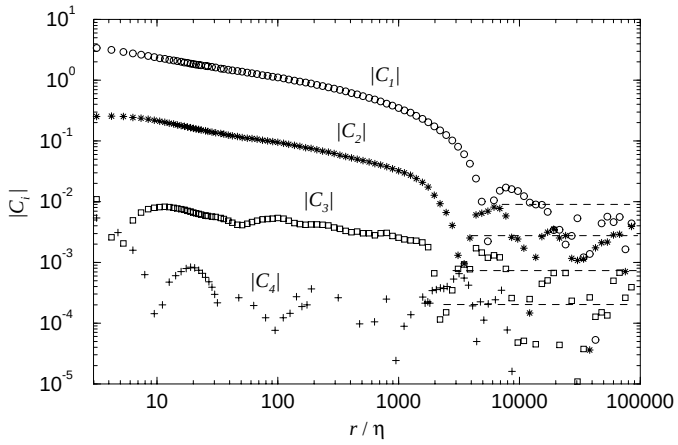

Fig. 2. Typical behaviour of the three first cumulants *versus* r/η in the air jet ($R_\lambda = 695$), for the longitudinal velocity increment.

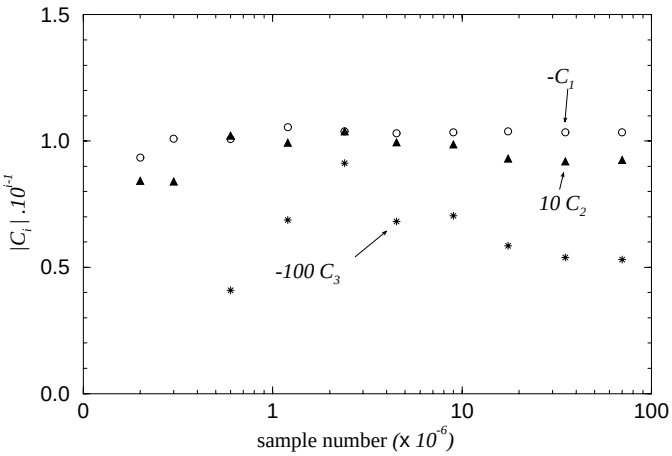

Fig. 3. Evolution of the cumulant values *versus* the data size. $-C_1$ (○), $10 \times C_2$ (▲), $-100 \times C_3$ (∗).

the fourth one is downed in the noise, leading to cumulants of order $p > 3$ negligible.

The three first cumulants of $\psi_{rl}(p)$ are, by definition, the three first centered moments of the G_{rl} distribution:

$$C_{1rl} = \langle \ln \alpha_{rl} \rangle$$
$$C_{2rl} = \langle (\ln \alpha_{rl} - \langle \ln \alpha_{rl} \rangle)^2 \rangle$$
$$C_{3rl} = \langle (\ln \alpha_{rl} - \langle \ln \alpha_{rl} \rangle)^3 \rangle$$

C_{1rl} represents the mean of $\ln(\alpha_{rl})$ and is linked to the ratio $\ln(\sigma_r/\sigma_l)$ (where $\sigma_r = (\langle \delta u_r^2 \rangle)^{1/2}$ Since α_r is less than 1, then C_{1rl} is negative. C_{2rl} is the variance of $\ln(\alpha_r)$ and is positive because velocity pdfs are flatter and flatter as r decreases from l to η. C_{3rl} is the third centered moment of $\ln(\alpha_r)$, it is negative and measures the deviation of G_r with the log-normal distribution.

Figure 2 shows that the absolute value of the third cumulant is small (about 10^{-2}), and in practice, these air jet data are typical of all our measurements. Therefore, all the cumulants presented in Section 3 have been estimated by a second order polynomial fit of $F_{rl}(p)$, defined as $F_{rl}(p) = \psi_{rl}(p)/p$, in such a way, a perfect linear behaviour of F_{rl} would mean a log-normal distribution for the multiplier α_{rl}. We observed that this fit, which gives $C_{prl} = 0$ for $p > 3$, leads to C_{3rl} more proportionnal to C_{1rl} and C_{2rl} (see Fig. 4) than the fifth order polynomial fit does in Figure 2.

It is observed that, for scales larger than a typical scale, hereafter called l_0, close to the integral scale L, the velocity increment pdf assumes a constant shape. Let us take it as the definition of l_0. The consistency of this definition will be shown later (end of Sect. 3.2). The experimental definition of the cumulants C_{irl} thus gives:

$$C_{irl} = C_{irlo} \quad \forall l \geq l_0.$$

It is natural to take l_0 as the reference scale in our data anlysis. In fact, experimentally, any scale l greater than l_0 gives the same cumulant values.

Hereafter, we denote by r the current scale ranging from η to l_0 and choose the reference scale l greater or equal than l_0, so l is no longer considered as a parameter, and we shall note $C_{irl} = C_i(r)$.

Since the cumulants $C_i(r)$ are the key quantities, we have checked their statistical convergences. Figure 3 displays the evolution of the cumulants values with the size of the data file (same flow as in Fig. 2). The statistical convergence is clearly reached, what is not surprising since the C_i values are obtained from velocity moments of order p ranging from $p = 0.6$ to $p = 6.6$. In particular, we observed that the convergence required by C_2 is nearly the same as that needed for the flatness factor based on the same scale. The above check of convergence has been performed on every flow.

2.3 The variational approach: a refinement of the KO62 model

In [1], the shape of the velocity increment pdfs is assumed to be the same at each scale. So, the multiplier α_r is no longer a random variable but a constant which value is given by the Kolmogorov law. Apart from the first one, all the cumulants are equal to zero, so [1] can be expressed as:

$$C_1(r) = \ln \frac{|\delta u(r)|}{|\delta u(l_0)|} = \frac{1}{3} \ln \left(\frac{r}{l_0} \right)$$
$$C_i(r) \equiv 0 \quad \forall\, i > 1.$$

The model proposed in [2,3] is an intermittency model which assumes a lognormal distribution for the multiplier α. So, all the cumulants beyond the second one are supposed to be equal to zero. Moreover, as in [1], a total scale invariance is assumed in this model and the scale l_0 is the only one taken as the characteristic scale of the flow. Therefore, it predicts a logarithmic law for the cumulant behaviour which can be true only in the limit of infinite R_λ and corresponds to:

$$C_1(r) \propto C_2(r) = -\mu_i \ln \left(\frac{r}{l_0} \right) \text{ with } \mu_i = \text{const. } i = 1, 2 \quad (4)$$
$$C_i(r) \equiv 0 \quad \forall\, i > 2. \quad (5)$$

On the contrary, the variational model takes into account the effect of the viscosity by introducing both the scale l_0 and the Kolmogorov scale η as characteristic scales. It predicts a power law behaviour instead of a logarithmic one and it induces a dependence on the ratio l_0/η for the cumulants. This means that this model predicts a dependence on the Reynolds number of the flow. The variational model predictions are [9,14]:

$$\mathrm{D}C_i(r) = \frac{\partial C_i(r)}{\partial \ln(r)} \propto r^{-\beta} \Leftrightarrow C_i(r) = k_i \left(\left(\frac{l_0}{r} \right)^{\beta} - 1 \right) \quad (6)$$

$$\text{and,} \qquad \beta \propto \frac{1}{\ln(l_0/\eta)} \Leftrightarrow \frac{1}{\beta} = \frac{1}{\beta_0} \ln \left(\frac{R_\lambda}{R_*} \right) \quad (7)$$

where β_0, k_i and R_* are constants. Hereafter, the derivative $\partial/\partial \ln(r)$ will be noted D.

2.4 ESS and proportionality of cumulants

ESS [8] can be tested in two different ways, which correspond to Figures 4a and b. Both are verifying the property (3). However, the range of validity limits are clearer in Figure 4a when comparing the variations in the range to out of the range.

On one hand, (3) is equivalent to the proportionality of the cumulants along the scales [7]:

$$(3) \Leftrightarrow C_i(r) = C_i[G_r] = n_r C_i[H] \quad \forall\, i$$

$$\Leftrightarrow \frac{C_i[G_r]}{C_j[G_r]} = A_{ij} \quad \forall\, i,j \quad (8)$$

where $C_i[G_r]$ is the ith cumulant of the considered distribution G_r and A_{ij} is not dependent on r.

Figure 4a shows typical behaviour of the ratios $-C_1(r)/C_2(r)$ and $-C_2(r)/C_3(r)$ *versus* $C_2(r)$ obtained with experimental data. These ratios are roughly constant, in comparison with the rapid departure from this constant value when going out of the range $0.4l_0 - 6\eta$.
On the other hand, from the equation (3), one also derives:

$$\ln\langle \alpha_r^p \rangle = n_r\, f(p) \Leftrightarrow \langle |\delta u(r)|^p \rangle = A_p \langle |\delta u(r)|^3 \rangle^{\zeta'_p}$$

which is, by definition, the characteristic property of ESS, $\zeta'_p = f(p)/f(3)$ being the scaling exponent of the absolute value velocity structure function of order p *versus* the third order one.

We observe, in Figure 4b, that it is very well verified by the same data in the same range of scales as for the proportionality of the cumulants. The lower limit (namely 6η) is in good agreement with the smallest scale (5η) reached with the generalization of the ESS [21]. The comparison between Figures 4a and 4b shows that neither of these two plots yields to clear edges of a plateau, even though the transition to the dissipation range is well seen on the former. Besides, Figure 4a displays raw data whereas, in Figure 4b, the quality of the demonstration depends on the adjustable parameters $f(2)$ and $f(4)$.

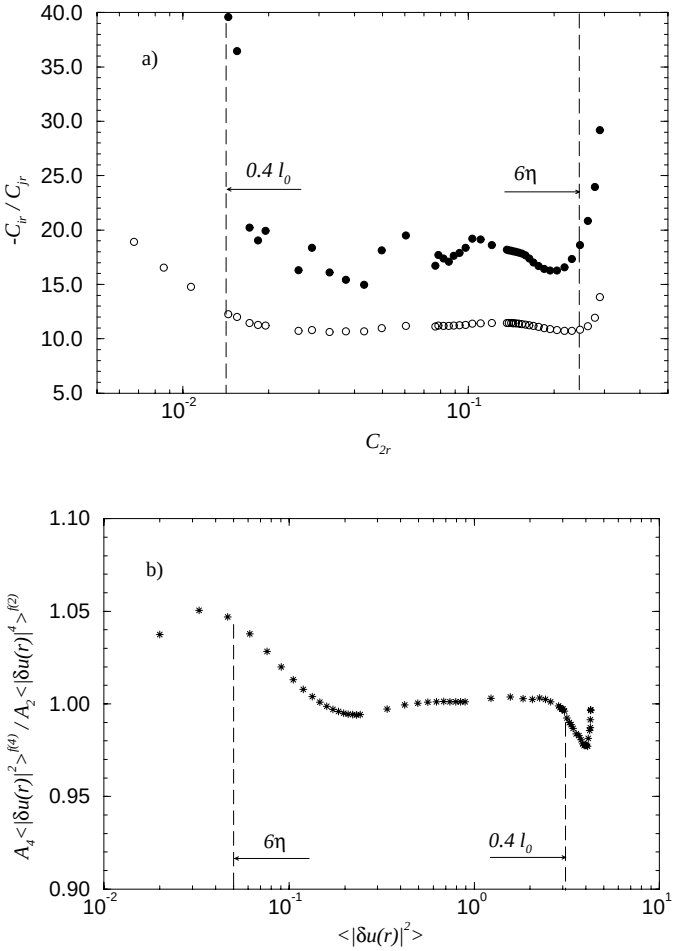

Fig. 4. (a) Behaviour of the cumulants ratios *versus* $C_2(r)$ for the turbulent air jet ($R_\lambda = 695$) in the longitudinal increments case; $-C_1(r)/C_2(r)$ (○); $-C_2(r)/C_3(r)$ (●). (b) Behaviour of the compensated quantity $\frac{A_4}{A_2} \frac{\langle |\delta u(r)|^2 \rangle^{f(4)}}{\langle |\delta u(r)|^4 \rangle^{f(2)}}$ *versus* $\langle |\delta u(r)|^2 \rangle$ for the tubulent air jet ($R_\lambda = 695$) in the longitudinal increments case.

This example, which is typical of all our experimental data, justifies the infinite divisibility hypothesis. It also shows that the proportionality of the cumulants (Fig. 4a) is experimentally a more stringent criterium than the self similarity of moments (Fig. 4b), even if they are formally equivalent.

3 Experimental results

3.1 Physical and numerical experiments

The measurements were made in four different turbulent flows. They are a cryogenic axisymmetric helium gas jet, and three air flows: an axisymmetric jet, a grid turbulence and the large wind tunnel of ONERA at Modane. The characteristics of these flows are presented in Table 1. In the helium jet, velocity measurements were obtained using a home made hot wire constant temperature anemometer [22]. Its unused characteristic is that the length

Table 1. Characteristics of the turbulent flows: U is the mean velocity, σ_u its r.m.s value, λ and η respectively the Taylor and the Kolmogorov length scales calculated as, $\lambda^2 = U^2\ \sigma_u^2/\langle(\mathrm{d}u/\mathrm{d}t)^2\rangle$ and $\eta = (\nu^2\ U^2\ /\ 15\langle(\mathrm{d}u/\mathrm{d}t)^2\rangle)^{\frac{1}{4}}$, f_s and f_k are respectively the sampling and the Kolmogorov frequencies.

	R_λ	U	σ_u	λ	η	f_s	f_k
		$\mathrm{m\,s^{-1}}$	$\mathrm{m\,s^{-1}}$	cm	mm	kHz	kHz
grid turbulence	144	19.6	0.64	0.35	0.15	45	22.5
air jet	350	1.68	0.44	1.28	0.33	45	0.80
	453	2.75	0.67	1.02	0.24	45	1.79
	695	6.29	1.55	0.67	0.13	45	7.57
Modane	2542	20.74	1.58	3.21	0.26	25	10.19
channel	3400	15.77	2.38	2.70	0.24	25	10.63
helium jet	352	0.35	0.075	0.033	9×10^{-3}	23	6.5
	703	1.6	0.3	0.0175	3.4×10^{-3}	272	75
	985	3.1	0.65	0.012	2×10^{-3}	368	250

of the sensitive part is a few times the diameter of the wire (10 μm *versus* 1.5 μm) giving a poor directivity to the measures [23]. For the air flows, velocity measurements were obtained with DISA 55M01 constant temperature system with Wollaston wire (3 μm diameter (d_w) and 0.35 mm length (l_w)) for all the air flows. In order to reduce averaging effects to a minimum, the ratio of wire length to Kolmogorov scale (l_w/η) was kept as small as possible ($1 < l_\mathrm{w}/\eta < 3$) and this, at the risk of difficulties which could arise when $l_\mathrm{w}/d_\mathrm{w} < 200$. However, the Wollaston wire, with $l_\mathrm{w}/d_\mathrm{w} \simeq 120$, gave consistent results with previous measurements made with a wire of $l_\mathrm{w}/d_\mathrm{w} > 200$ while the measurement location is far from any boundary [24]. In the case of the ONERA wind tunnel, a cold wire (home built constant current anemometer) was also used to measure temperature fluctuations simultaneously with hot wire signals in order to separate velocity fluctuations (for details see [25]).

Longitudinal velocity increments $\delta u_\parallel(r)$ were obtained with the measurement of the streamwise velocity component u by using a single hot wire. The time-space conversion has been done by using the Taylor hypothesis. We have used a particular time-space method, namely, $\delta x = -u(t)\delta t$, where $u(t)$ is the instantaneous streamwise velocity component, instead of a constant mean velocity U as it is usually done. All the results presented below were obtained by using this particular time-space conversion, which is detailed in [15,26]. The best spatial and temporal resolution of the longitudinal increments is at a range of twice or three times the Kolmogorov scale η, thus missing a significant part of the dissipation range.

Transverse velocity increments $\delta u_\perp(r)$ were performed in the jet and in the grid by measuring the transverse velocity component v. The use of time-space conversion permits to obtain the transverse increments of the transverse velocity component $\delta v(x)$. The resolution of the transverse velocity gradients is limited either by the X array size or the signal to noise ratio.

Table 2. Parameters of the numerical simulations: N is the size of the simulations, t/T is the total run time in eddy turnover units. The energy dissipation rate ϵ has been adjusted to achieve the numerical resolution $k_\mathrm{max}\eta = 2$.

R_λ	N	$\epsilon L/{\sigma_u}^3$	t/T	L/η
63	128	0.80	9.3	52
142	384	0.73	5.9	162.06
168	512	0.69	5.9	197.34

Each file contains 70×10^6 samples which are sufficient to reach a reasonable statistical convergence of the statistical moments $\langle[\delta u_{\parallel,\perp}(r)]^p\rangle$ until the order $p \simeq 6$.

The DNS data kindly given by Jiménez, have been carried out in [27]. These DNS are essentially the same as in [18]. Their main characteristics are summarized in Table 2. Both longitudinal and transverse velocity increments have been calculated at twelve different scales logarithmically distributed over the whole scale range. Pdf have been calculated with about 400×10^6 samples.

3.2 Relative behaviour of cumulants

We are able to characterize the G_{rl_0} (hereafter G_r) distribution at each scale r by its cumulants. We shall first verify again the infinite divisibility of the G_r distributions in a slightly different way than in Section 2. Then, the universality of the result, the viscous cut off scale and the definition of the scale l_0 will be discussed.

Figure 5 shows the mutual behaviour of the C_{1r} and C_{2r} cumulants obtained from longitudinal velocity increments measured both in the helium jet, and in air experiments. The results appear relatively grouped, roughly linear, up to a plateau (not reached in the Modane channel flow) which can be interpreted as the velocity gradient pdf shape.

In the case of the Modane data file ($R_\lambda = 2542$), we discovered a stationary problem in the velocity signal due to brief and periodical openings of the channel air entries which have caused strong inhomogeneities in the mean flow and spoiled the whole statistics. The experimental data shown in Figure 5 have been obtained from 1.5×10^7 points corresponding to the longest signal duration between two openings. Note that the convergence study we performed (Fig. 3) ensures the validity of the results obtained with such a partial sample. Even if we have observed that the cumulants are sensitive to fluctuating conditions of homogeneity and isotropy, we are not able to quantify this influence.

At small scale, the intersection of the cascade range linear fit with the plateau which defines the viscous cut off scale, is rather clean-cut compared to the progressive transition from the inertial range to the viscous one. Indeed, in the helium experiments, we can study the behaviour of this viscous cut off scale with the Reynolds number. It goes

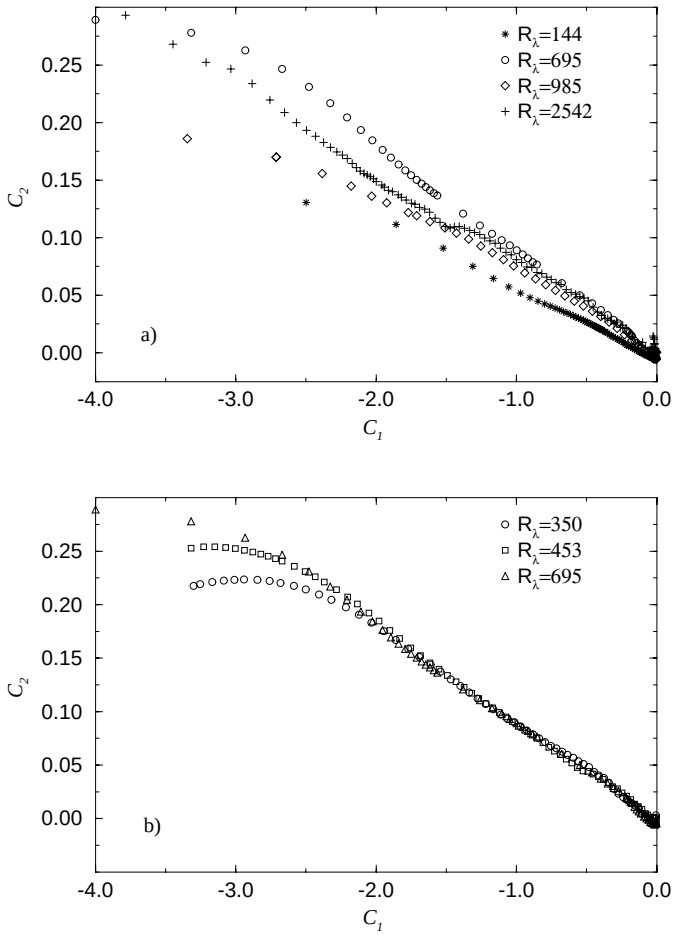

Fig. 5. Behaviour of C_2 *versus* C_1; (a) for different setups: grid ($*$), air jet ($\circ$), helium jet ($\diamond$), Modane channel ($+$); (b) only in the air jet (*cf.* Tab. 1).

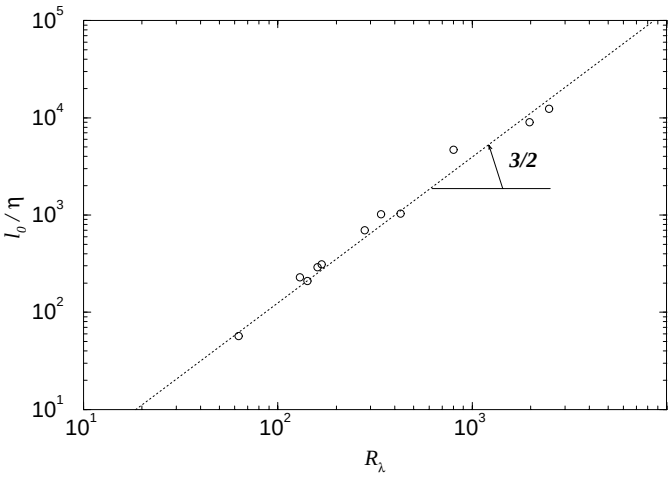

Fig. 6. Behaviour of l_0/η *versus* R_λ for longitudinal increments; measured values ($\circ$), dotted line: $l_0/\eta \simeq R_\lambda^{3/2}/8$.

as $R_\lambda^{-3/2}$ as η does, up to the $R_\lambda = 703$ run. For larger R_λ, the viscous cut off is at a constant value, showing the limitation of the home made anemometer used in the helium jet. For $R_\lambda \leq 703$, this scale corresponds to 3.3η. It is interesting to notice that the value of $\mathrm{D}(\ln|\delta u^3|)$ at this scale is approximately 2.6, that is closer to the dissipative value 3 than to the inertial value 1.

Let us now comment on the universality of the slope $\mathrm{d}C_2/\mathrm{d}C_1$. We think that the difference between the slopes shown in Figure 5a is significant. Indeed, for a given experiment (Fig. 5b) the slopes are equal for different Reynolds numbers, even with several years between measurements. On the contrary, different experiments of the same type, in particular for the two jets, yield to different slopes (Fig. 5a). This is why, we do not give any universal value for this slope; note, however, that values we found are around $\mathrm{d}C_2/\mathrm{d}C_1 = 0.08$, in rough agreement with the wavelet analysis of [28].

These results are somewhat different from those obtained in [21]. Figure 5a suggests that the ESS is verified in all the types of flow including mean sheared flows, on the contrary, Benzi *et al.* [21] did not find any ESS for flows enclosing a shear. Moreover, the different slopes observed, in Figure 5a, is contrary to the universality of scaling exponents obtained by these authors. Indeed, we observe a non dependency on the Reynolds number (Fig. 5b), but only for a given flow.

A slope independent on the Reynolds number allows to safely extrapolate towards infinity Reynolds number limit and to define the scaling exponents:

$$\zeta'_p = f(p) \simeq \frac{p}{3}\left(\frac{C_1 + C_2 p/2}{C_1 + 3C_2/2}\right).$$

Different slopes depending on experimental setups mean different ζ'_p which would not be universal. This result seems contradictory to the universality of velocity scaling exponents which have been measured in a lot of experiments. In fact, the differences induced between various experiments are of the order of the error bars given on usual compilations (see, for instance, [29]). This imprecision on ζ'_p thus would not be due to a lack of accuracy of data but would be intrinsic to the diversity of experimental setups.

Finally, let us remark that the proportionality of C_2 *versus* C_1 down to the smallest values gives all its meaning to the definition previously proposed for the large scale l_0 (Sect. 2.2). The scale where C_2 reaches zero is clearly the same as the one where C_1 does. Figure 6 shows that l_0/η scales as $R_\lambda^{3/2}$ as for the classical integral scale L. In all air experiments (grid, jet and Modane channel), the ratio l_0/L has been found constant and nearly equal to 3, (the integral scale L being estimated with the velocity correlation curve).

Concerning the third cumulant, our experimental data suggest that the C_3 values are very small (*cf.* Fig. 2), nevertheless, we checked its proportionality with C_2 and C_1, at least, in the flows where the signal to noise ratio was large enough (see [15,22]).

3.3 Estimator β

Since the cumulants are roughly proportional at any scale ranging from $0.4l_0$ to 6η, their behaviour can be examined by only studying the first one C_1.

In Section 2.3, we have seen that the lognormal model and the variational approach give two different predictions for the dependence of C_1 *versus* r. Figure 2 clearly shows that the former prediction (5) is not verified by experimental data. The latter one is expressed by (6) and can be tested in two different ways:

- A soft way is to consider it as a parameterization of finite Reynolds number effects and of the resulting departure from the power law dependence of velocity moments ($\ln(r)$ behaviour for C_1). The question is then to look if an equation like (6) can reasonably reproduce the experimental C_1 behaviour. This is the spirit of the analysis of [28]. They showed that a power law behaviour for C_1 gives a much better agreement with experimental data than a $ln(r)$ behaviour. As shown in Figure 7, our data are also very well fitted by (6) where additive constant k_1 and the exponent β are adjustable parameters, experimentally estimated with a least squares method.
- A stricter point of view is to look if, among all the possible departures from the $\ln(r)$ behaviour, (6) is a good one on the whole inertial range. This should allow, inter alia, to determine unambiguously the parameters β and k_1.

As we have:

$$(6) \quad \Rightarrow \quad \mathrm{D}C_i = \frac{\partial C_i}{\partial \ln(r)} = -\beta(C_i + k_i)$$

a systematic test is to plot $\mathrm{D}C_1$ *versus* C_1 as shown in Figure 8a.

For small R_λ ($R_\lambda < 400$) the linear fit appears as a good one, in many cases within the experimental accuracy. It expresses that the influence of viscosity goes up to the largest scale.

For large Reynolds numbers, deviations from linear behaviour are systematically out of the experimental error bars. The range of scales influenced by the viscosity no more extends up to the integral scale. For these large Reynolds numbers, the prediction (6) appears as a simplification which no longer captures the detailed behaviour of the cumulant C_1. In the present state of the art, however we prefer to take a conservative point of view, closer to the soft way previously mentioned. The reason is that an experimental derivative is a delicate procedure which could enhance unexpected artefacts. As we have seen previously (Fig. 7) a single parameter β well integrates the continuous variation of $\mathrm{D}C_1$, without any real plateau, from large to small scales.

Again we do not pretend that Figure 8 justifies the law proposed in equation (6). On the contrary, the fit of the data by a straight line aims at determining objectively the best global parameter β. We have thus to use a wide range for this fit which we systematically choose between $0.4l_0$ and 15η.

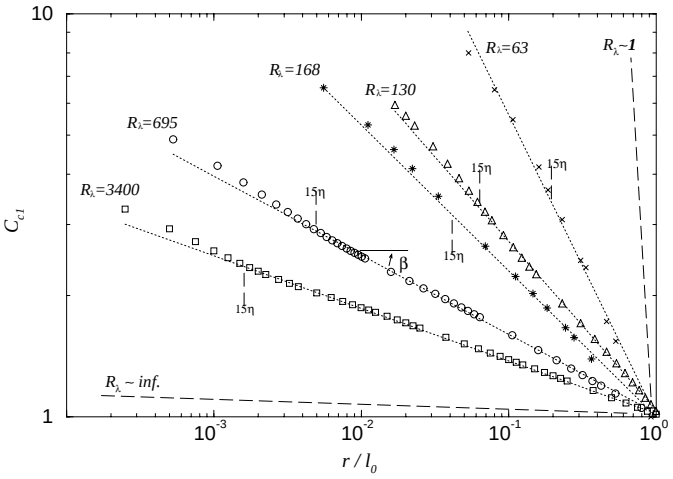

Fig. 7. Behaviour of $C_{c1}(r) = (C_{1r}/k_1 + 1)$ *versus* r/l_0 in the longitudinal increments case for several types of flows; Modane wind tunnel at $R_\lambda = 3400$ (□); turbulent air jet at $R_\lambda = 695$ (○); homogeneous isotropic turbulence DNS 512^3 at $R_\lambda = 168$ (∗); grid turbulence at $R_\lambda = 130$ (△); homogeneous isotropic turbulence DNS 128^3 at $R_\lambda = 63$ (×); power fit (dotted line).

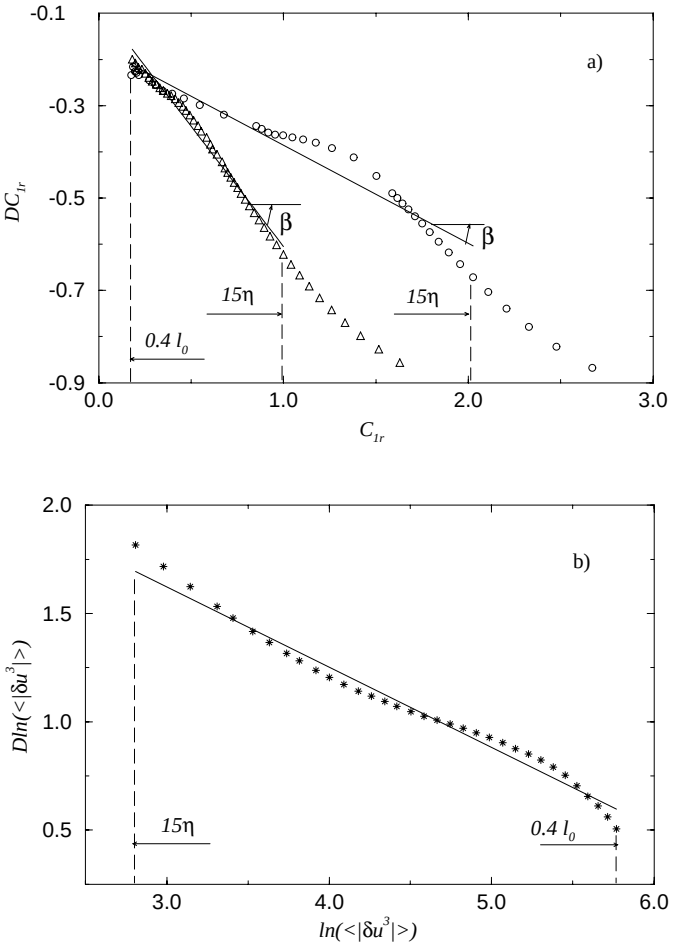

Fig. 8. (a) Behaviour of $\mathrm{D}C_{1r}$ *versus* C_{1r}: air jet at $R_\lambda = 695$ (○), grid at $R_\lambda = 144$ (△), linear fit (line). (b) Behaviour of $\mathrm{D}\ln(\langle|\delta u^3|\rangle)$ *versus* $\ln(\langle|\delta u^3|\rangle)$ in the helium jet at $R_\lambda = 352$ (∗), linear fit (line).

Since the cumulants are proportional, it is also possible to estimate the β exponent directly from the $|\delta u_r|$ moments:

$$\psi_r(p) = \left(\left(\frac{l_0}{r}\right)^{\beta} - 1\right)\left(k_1 p + k_2\frac{p^2}{2} + ... + k_i\frac{p^i}{i!} + ...\right)$$

$$\Rightarrow \mathrm{D}\ln\langle|\delta u_r|^p\rangle = \frac{\partial \ln\langle|\delta u_r|^p\rangle}{\partial \ln(r)}$$

$$= -\beta(\ln\langle|\delta u_r|^p\rangle + \kappa_p)$$

$$\text{with, } \kappa_p = \left(k_1 p + k_2\frac{p^2}{2} + ... + k_i\frac{p^i}{i!} + ...\right) - \ln\langle|\delta u_{l_0}|^p\rangle.$$

Figure 8b shows the typical behaviour of $\mathrm{D}\ln\langle|\delta u_r|^p\rangle$ *versus* $\ln\langle|\delta u_r|^p\rangle$, in the case of $p = 3$, obtained from the helium jet data.

We observe a behaviour similar to $\mathrm{D}C_1(C_1)$. We have verified that the shape of the $\mathrm{D}\ln|\delta u_r|^p$ does not depend on p (not represented here) according to the previous relation. In each case (Fig. 8), we only plotted the range where the cumulants are proportional, namely, $6\eta - 0.4l_0$, that is all the range where the multiplicative cascade is active, but, as said above, the average slope β has only been estimated on the range $15\eta - 0.4l_0$.

Figure 7 gathers the behaviour of the first compensated cumulant Cc_1 for several flows, defined as: $Cc_i(r) = (C_{ir}/k_i + 1)$. Scaling power laws are observed from the end of the dissipation range to the largest scale l_0 in agreement with the variational prediction (6).

This figure also gives an idea of the β exponent behaviour with the Reynolds number. As R_λ increases, β decreases and tends to zero in the limit of infinite Reynolds number. In this case, the variational model is equivalent to a $\ln(r)$ behaviour that is the so called third hypothesis of the Kolmogorov-Obukhov 62 model [2,3]. On the opposite, at small R_λ, β increases and tends to infinity at R_λ of order 1. Since β is the average rate of variation of the cumulant along the scales, it can be interpreted as the "speed" at which the pdf changes from a Gaussian shape to an exponential one along the scales. In other words, it is a global statistical estimator which means, in average, the "acceleration" of the intermittency cascade process along the scales.

3.4 Transverse velocity increments

Before going into the same analysis for transverse increments as for the longitudinal one, let us refer to a controversy about comparison of their intermittency based on the structure function [30,31]. In Figure 9, is displayed the derivative (*versus* the logarithm of the scale r) of the logarithm of the sixth order structure function for both transverse and longitudinal velocity increments for the air jet at $R_\lambda = 695$. We observe that an horizontal shift of a factor 2.2 makes the data to almost coincide. On the sole basis of these structure functions, it seems thus difficult to invoke a difference between the intermittency exponents. Concerning the scale dependence of C_i cumulants, we notice that the determination of large scale $l_{0\perp}$ for transverse

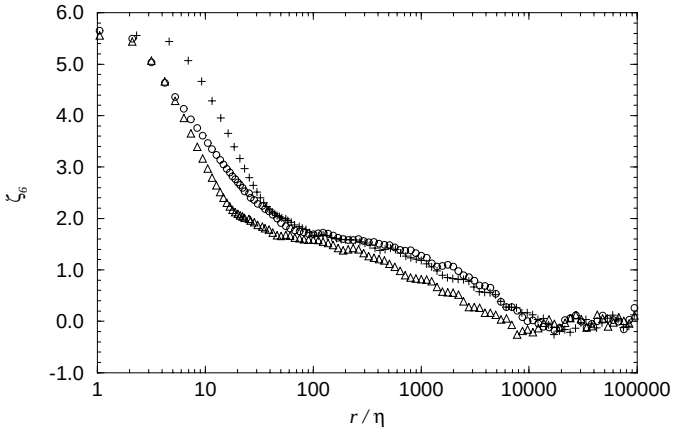

Fig. 9. $\zeta_6 = \mathrm{D}[\ln(\langle|\delta u(r)|^6\rangle)]$ *versus* r measured in the air jet ($R_\lambda = 695$); ($\circ$) longitudinal increments, ($\triangle$) transverse increments and ($+$) same transverse increments shifted of a factor 2.2

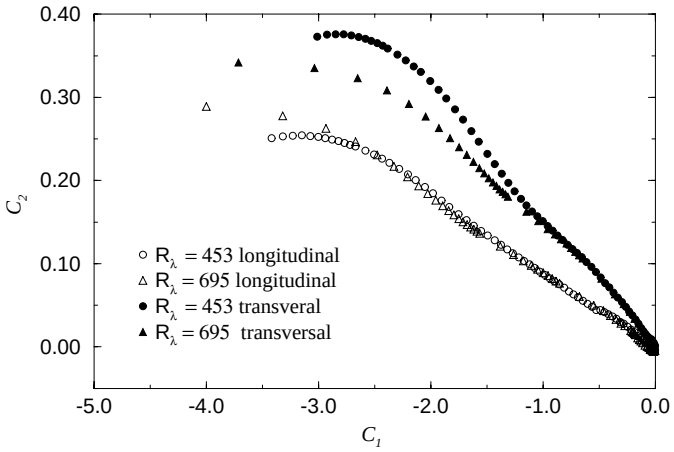

Fig. 10. Behaviour of C_2 *versus* C_1 in the longitudinal and in the transversal increments cases for the jet.

increments gives systematically half the value obtained from the longitudinal ones, in accordance with the shift invoked above.

In Figure 10, we compare the behaviour of C_2 *versus* C_1 for transverse and longitudinal data for the air jet experiment for two different Reynolds numbers. We first observe a clear difference between the two types of increments. Besides, the merging of transverse increments data for different Reynolds numbers is less obvious than for the longitudinal case. Indeed, a systematic tendency appears in all our results where transverse C_2 values for a given C_1 decreases and tends to the longitudinal one when R_λ increases. Let us note that, for a given flow, an increasing of R_λ always improves isotropy (estimated with the ratio u'/v'). This could be connected with the remarks of L'vov *et al.* [32]. They argued that, within homogeneity and isotropy, a difference in scaling between longitudinal and transverse velocity moments can only appear for order larger than 4. Our approach is first concerned with absolute values of velocity differences, and second to the limit of vanishing order p. In this context, if we assume that

for a given order the intermittency exponents of the longitudinal and transversal increments are the same, then the difference of scaling observed in Figure 10 could be attributed to a lack of homogeneity or/and isotropy.

4 Intermittency and Reynolds number

In order to test the robustness of the β estimator, the data cumulant analysis has been applied in several physical and numerical experiments for a large range of Reynolds numbers (see Tabs. 1 and 2).

4.1 Universal β behaviour with R_λ:

Figure 11 gives the β exponent values measured with the longitudinal velocity increment. As already observed in the previous paper [15], physical data, shown in Figure 11, roughly agree with the second prediction of the variational model (7) on about two decades of R_λ. Actually, experimental points merge on a weakly bent curve, however in first order, $1/\beta$ behaves linearly with R_λ. The error bars take into account a possible uncertainty in determining l_0 and η. We thus varied the fitting range in Figure 8, keeping its length constant in logarithmic coordinates, within $\pm 20\%$ for l_0. These data of β *versus* R_λ also agree with a power law behaviour (not shown in this paper). However, in our knowledge, there is no argument to justify such a dependence.

Note that in [12] a similar figure presents the evolution of an exponent β *versus* R_λ. It corresponded to a power law $C_2 = k_2(r/l_0)^{-\beta}$ (without additional constant) which fitted a narrower range of the measured dependence of C_2 *versus* r. The result of the present paper is that, within the cautions quoted above, and with the additional constant, the power law can reasonably fit most of the range (Fig. 8), which yields us to redefine the β estimator (7) in this scope.

In Figure 11 are also plotted numerical data, in particular, it is interesting to compare the DNS of [18] with the grid turbulent flow which has nearly the same Reynolds number. They yield very close values of the β exponent.

In Figure 12, transverse velocity increments have been added (both numerical and physical experiments). All the data collapse on the same universal curve which means that β is not dependent on the velocity increment type. That result is not so surprising, since our analysis is based on the absolute value of δu_r, avoiding any skewness effect. Nevertheless, this result is important since there is no theoretical prediction on it.

As a whole, the best logarithmic fit of experimental data is:

$$\frac{1}{\beta} \simeq \frac{1}{0.28} \log\left(\frac{R_\lambda}{28}\right).$$

All these results show the intrinsic ability of the β estimator to quantify the global effect of intermittency along scales, and to generalize its universal behaviour with R_λ to all increment data types.

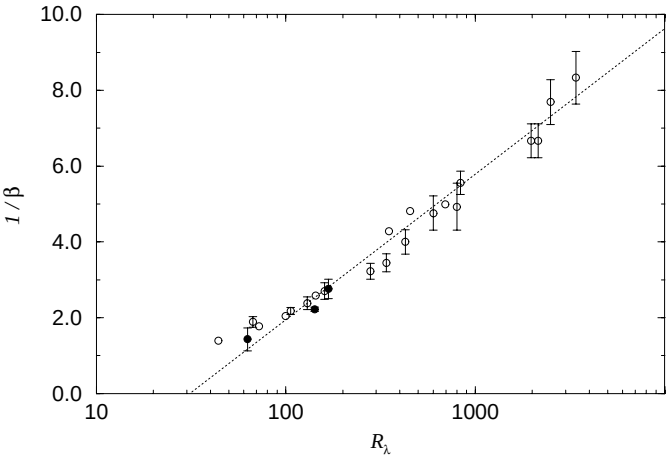

Fig. 11. Behaviour of $1/\beta$ *versus* R_λ in the longitudinal increments case; physical experiments (○); DNS (●); logarithmic fit (dotted line). The errors bars are obtained by varying the fitting range of scales.

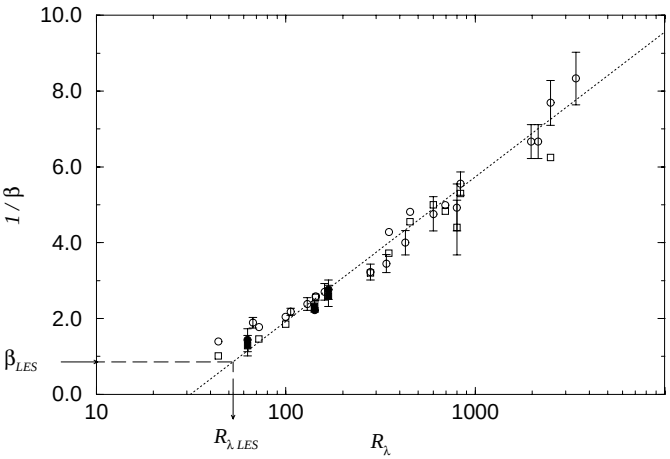

Fig. 12. Behaviour of $1/\beta$ *versus* R_λ both for transverse and longitudinal increments; longitudinal increment: physical experiments (○), DNS (●); transverse increment: physical experiments (□), DNS (■).

4.2 Cascade multiplier dependence with R_λ:

The β exponent permits to characterize how the cumulants $C_i(r)$ evolved along the scales. Their absolute values or their ratio depend on the behaviour of the k_i prefactors *versus* the Reynolds number as defined in (6). There is no theoretical prediction for these factor values. Figure 13a (resp. 13b) clearly shows, in average, a linear dependence of k_1 (resp. k_2) with $1/\beta$. In Figure 13b, the dispersion of data corresponds to the flow type dependence revealed in Figure 5.

Experimental data fits lead to:

$$k_1 = \frac{\mu_1}{\beta} \qquad \text{with,} \quad \mu_1 = -0.22 \pm 0.04$$

$$k_2 = \frac{\mu_2}{\beta} \qquad \mu_2 = 0.016 \pm 0.003.$$

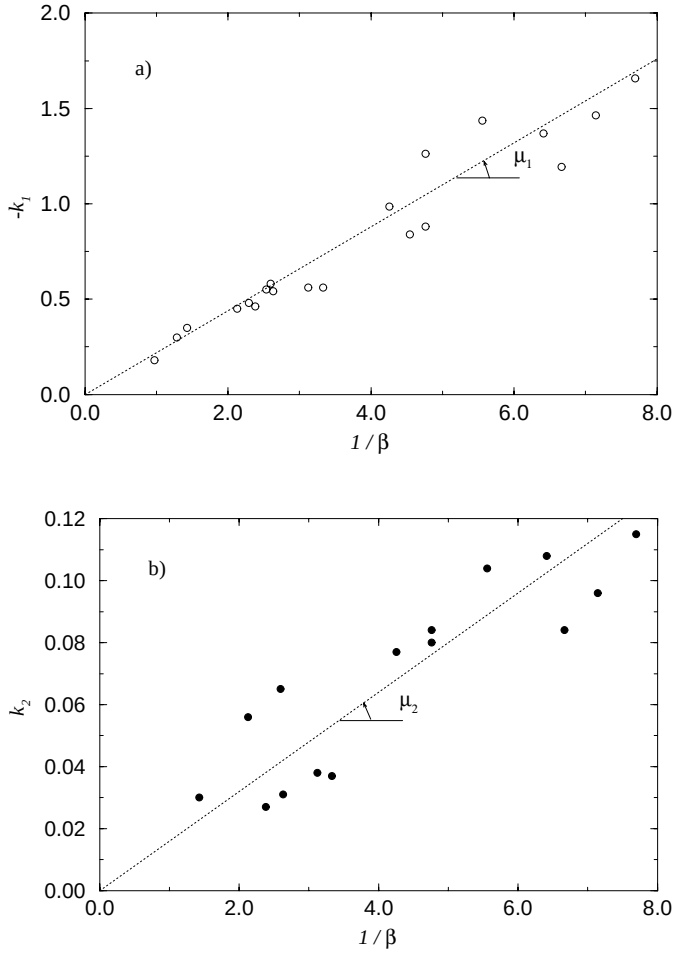

Fig. 13. Behaviour *versus* $1/\beta$ of: (a) $-k_1$ both for transverse and longitudinal increments; (b) k_2 for longitudinal increments.

In the infinite Reynolds limit, β tends to zero, thus (6) becomes:

$$C_{ir} = k_i \left(\left(\frac{l_0}{r} \right)^{\beta} - 1 \right) \simeq \beta\, k_i \ln \left(\frac{l_0}{r} \right) \Rightarrow C_{1r} \simeq \mu_1 \ln \left(\frac{l_0}{r} \right)$$
$$C_{2r} \simeq \mu_2 \ln (l_0 r)\,.$$

According to the Kolmogorov theory [1], we expect a μ_1 value close to $-\frac{1}{3}$. The observed difference is due to the fact that DC_1 depends on the scale.

Otherwise, the μ_2 value seems reasonable, according to the Refined Similarity Hypothesis: $\epsilon_r \sim (\delta u(r))/r^3$. Since $\langle (\ln(\epsilon_r))^2 \rangle \simeq 9 \langle (\ln(\delta u))^2 \rangle$, (where μ is the intermittency constant of ϵ_r), we can expect that $\mu \simeq 9\mu_2$. From this point of view, $\mu_2 = 0.016$ is not in contradiction with the well accepted $\mu \simeq 0.18 - 0.25$.

Therefore, Figures 12 and 13a show that each cumulant $C_i(r)$ only depends on one constant μ_i and the statistical estimator $\beta(R_\lambda)$.

5 Asymmetry of the longitudinal increments

The whole analysis above only refers to the symmetric part of velocity increments pdf, whereas, as it is well known, the dissipation power ϵ is related to the asymmetric part of the longitudinal velocity increments pdf:

$$\langle \delta u_l^3 \rangle \simeq -\frac{4}{5} \epsilon r.$$

However, it is a common belief that the signed and absolute odd moments of δu_l behave in the same way. In particular, it is generally assumed that the ratio $\langle \delta u^3 \rangle / \langle |\delta u^3| \rangle$ has a universal value in the inertial range. This is to be expected, indeed, in the frame of the Kolmogorov Refined Similarity Hypothesis.

The high statistics we use (about 10^4 integral times) ensure good convergence for the signed third moment. We thus have studied the behaviour of what can be called the asymmetry:

$$A(r) = -\frac{\langle \delta u^3 \rangle}{\langle |\delta u^3| \rangle}$$

versus the scale for different Reynolds numbers (Fig. 14). The ratio $A(r)$ is indeed a better measure of the asymmetry of the pdf than the skewness:

$$S(r) = -\frac{\langle \delta u^3 \rangle}{\langle \delta u^2 \rangle^{3/2}}$$

as the latter is sensitive to the phenomenon of intermittency, *i.e.* the change of shape of the pdf.

Before to look at the results, let us point that a constant value of $A(r)$ in the inertial range would ensure to comfortably answer a dilemma in the literature. On the one hand, many authors pretend that the gradient skewness S_η, which is the small scale limit of $S(r)$, grows as the Reynolds number increases. On the other hand, it is often claimed that the one dimensional velocity spectrum $E(k)$ has a universal shape at the viscous cut off that is $\eta/\nu^2 E(k)$ is a universal function of $k\eta$. The latter result implies a universal value for S_η and thus is contradictory to the former one.

However, from Section 3, we know that:

$$\frac{S_\eta}{A(\eta)} = \frac{\langle |\delta u^3| \rangle}{\langle \delta u^2 \rangle^{3/2}} (\eta)$$
$$= \frac{\langle |\delta u^3| \rangle}{\langle \delta u^2 \rangle^{3/2}} (l_0) \exp(\frac{3}{2} C_2(\eta))$$

in the log-normal approximation. The first function is universal, being controlled by the Gaussian nature of velocity fluctuations at large scale. The second factor grows when R_λ increases, for a given experiment. Thus, either $A(\eta)$ is universal and S_η goes up with R_λ, or S_η is a constant and $A(\eta)$ goes down.

Figures 14a, b give the result for $A(r)$. This ratio is not strictly constant, but it never uniformly decreases when going down the scales. Thus, the above conclusion is valid as $A(r)$ cannot asymptotically be larger than 1.

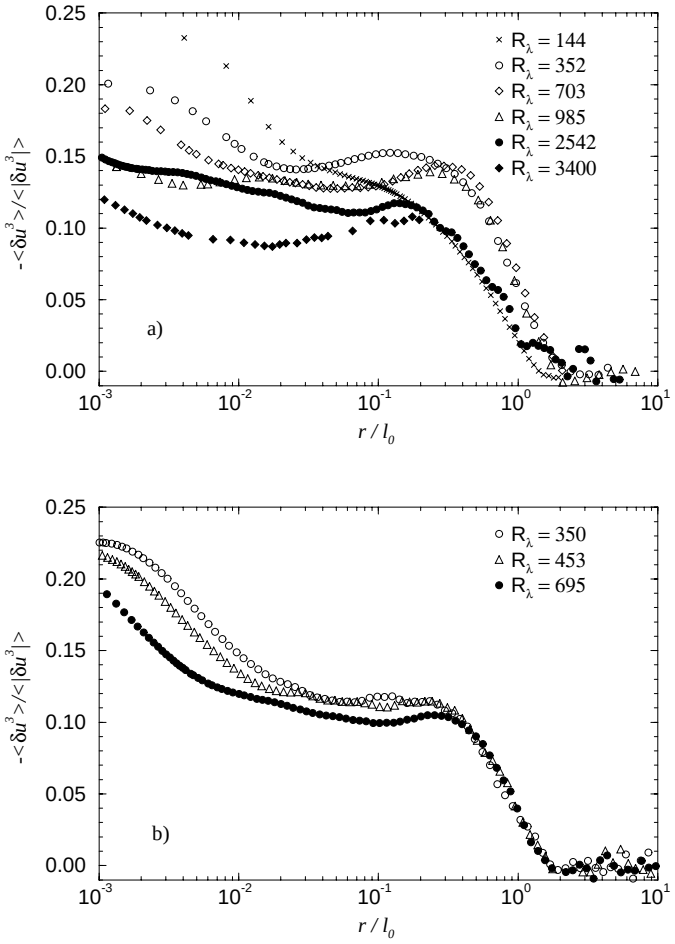

Fig. 14. Behaviour of $A(r) = -\langle \delta u^3 \rangle / \langle |\delta u^3| \rangle$ *versus* r/l_0 for different flows: (a) grid ($\times$), helium jet ($\circ$, $\diamond$, $\triangle$), Modane ($\bullet$, $\blacklozenge$); (b) air jet.

At first sight, one could conclude that $A(r)$ has a universal value at large scale except for the helium experiment. However we had better look at each experiment independently at a thiner level. Then, as it can be seen already in Figure 14a for the helium experiments, and in Figure 14b for the air jet experiments, a systematic decrease of A when Reynolds grows is visible.

While we are confident in the systematic character of this result, it affords for cautions verification. Indeed, first, it allows for a constant value of the gradient skewness S_η, as the decrease of $A(r)$ is of the good order of magnitude. Secondly, if extrapolated to very large Reynolds (rather unphysical on terrestrial grounds, but conceptually important) it opens the possibility that $A(r)$ goes to zero as Reynolds goes to infinity. In the inertial range $A(r)$ is, within a 4/5 factor, equal to the ratio of ϵ to $\langle |\delta u|^3 \rangle / r$. It would mean that the dissipation goes to zero when compared to the only inertial quantity to which we can. In this way, turbulence would be "non dissipative" in the infinite Reynolds limit.

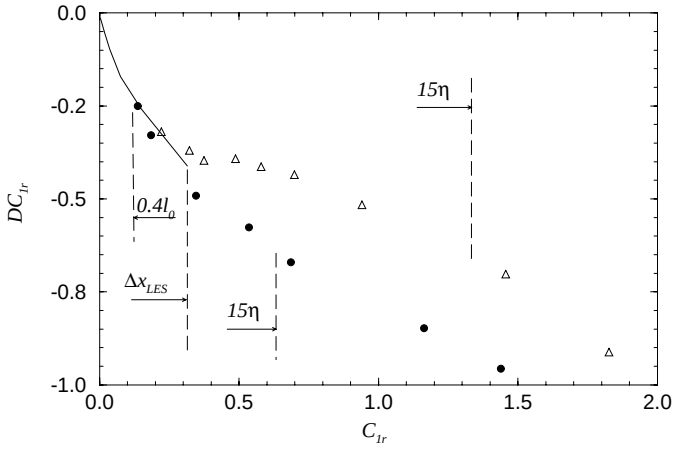

Fig. 15. Behaviour of $DC_1(r)$ *versus* $C_1(r)$ obtained in DNS ($R_\lambda = 63(\bullet)$, $R_\lambda = 168(\triangle)$) and in a 128^3 LES (solid line).

6 An application to the LES

The previous sections strongly suggest that β behaves monotonously with R_λ, whatever the type of flow or the numerical simulation is. Therefore, it is possible to estimate the Reynolds number based on the Taylor microscale from the knowledge of β. This can be useful, particularly in the case of Large Eddy Simulation. The use of a subgrid modelling prevents from knowing the effective dissipative scale, and therefore from calculating R_λ. Indeed, in most of LES, the Reynolds number is often estimated by a large scale property of which the Reynolds number is *a priori* known ([33] and references therein).

Figures 8 clearly show that the slope β is well defined until the largest scale l_0, which means that the part of the largest inertial scales only can be sufficient to estimate it. This property is especially interesting at small and moderate Reynolds numbers, and we tried to use it on a LES performed by Métais and Lesieur [34] on a 128^3 periodic grid with a subgrid modelling based on the Smagorinsky's model [35]. Transverse velocity increments have been calculated at ten different separations respectively equal to 2, 3, 4, 5, 6, 8, 10, 12, 14 and 16 times the mesh size $\Delta x_{\rm LES}$. Each pdf has been obtained with 12×10^6 data, and the previous cumulant analysis yields ten C_1 values. In this case, the reference scale l_0 has been found equal to $6\Delta x_{\rm LES}$. The slope $\beta_{\rm LES}$ has been determined with ranges of different extents included in the range 2-6 meshes (equivalent to $0.4l_0$ - $\Delta x_{\rm LES}$ in Fig. 15), leading to the value $\beta_{\rm LES} = 1.1$ with an error bar of 0.1. Therefore, the universal curve $\beta(R_\lambda)$ leads to an approximative Taylor Reynolds number of $R_{\lambda \rm LES} \simeq 50$ (see Fig. 12). It is, *a priori*, surprising to notice that this LES leads to a $R_{\lambda \rm LES}$ value smaller than this obtained with the 128^3 DNS ($R_{\lambda \rm DNS} = 63$).

In order to understand this result, we have to compare the range of scales which are actually simulated in each case. In the DNS, by definition, all the scales of the flow are calculated and so, the energy injection scale is chosen to be of the order of the box size, as it is sketched in Figure 16.

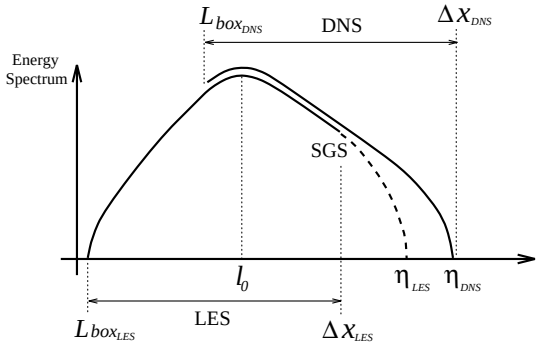

Fig. 16. Sketch of LES and DNS spectra.

On the opposite, the objective of the LES is to study the large scale structures so that this injection scale is chosen one order below the box size, and the mesh size is assumed to be in the inertial range, but the ratio $\Delta x_{\rm LES}/\eta_{\rm LES}$ is unknown.

In the present case, the numerical data base of the LES and DNS leads to:

$$\frac{l_{0\rm LES}}{\Delta x_{\rm LES}} \simeq 6$$
$$\frac{l_{0\rm DNS}}{\eta_{\rm DNS}} \simeq 50 \quad \text{with} \quad \frac{\Delta x_{\rm DNS}}{\eta_{\rm DNS}} \simeq 1.44.$$

Assuming that the ratio $\Delta x_{\rm LES}/\eta_{\rm LES}$ only depends on the subgrid scale modelling and not on the Reynolds number, we can estimate it by using the experimental relation displayed in Figure 6 ($l_0/\eta \simeq R_\lambda^{3/2}/8$). It yields:

$$\Delta x_{\rm LES} \simeq 6.4\,\eta_{\rm LES}.$$

A way to test the efficiency of this subgrid modelling is to consider the LES with the same $L_{\rm box}/l_0$ ratio as in the DNS and to compare their Reynolds numbers. In terms of Reynolds number, by using again $R_\lambda \sim \eta^{2/3}$, the above relation involves a ratio of

$$\frac{R_{\lambda\rm LES}}{R_{\lambda\rm DNS}} \simeq 2.7.$$

This example suggests that usual LES with a Smagorinsky's model are able to reach more than double the Taylor Reynolds number of DNS with the same numerical grid size.

7 Concluding remarks

The evolution of velocity increments distributions, which we rely, as most of the authors do, to a multiplicative cascade, can be described as the repetitive action of a propagator. The rate of progression of the cascade along the scales, or the shape of the propagator which ensures it, are two different problems. The experimental data analysed, in this paper, with the cumulant technic show that the former exhibits a universality which seems not to be present in the latter. Indeed, universality can be understood in three different ways: along the scales, *versus* the Reynolds number and for different experimental setups. On one hand, the shape of the propagator, as characterized by the C_2/C_1 ratio, exhibits differences between experimental setups, even for a same type of flow (Fig. 5a). However, this ratio is constant within an experimental setup, along the scales and *versus* the Reynolds number (Fig. 5b). On the other hand, the progression of the cascade, measured, for instance, by the C_1 cumulant, is not regular as assumed in the scale invariant models. That is, the same step in the cascade does not mean the same ratio in scales all along the range (Figs. 8a, b). The corresponding "acceleration" can be measured by the global β estimator. However, the relation between β and Reynolds does not depend on the experimental setup, nor on the type of flow, and is verified as well with Direct Numerical Simulation (Fig. 12). It allowed us to estimate the R_λ of a Large Eddy Simulation.

Another important result of the paper is the pertinence of the scale where the cascade begins (l_0 scale). Its determination is easier and sharper than for the integral scale. The relation between l_0/η and R_λ is universal for longitudinal increments: $l_0/\eta \simeq R_\lambda^{3/2}$ (Fig. 6). Transverse increment defines its own l_0 scale different from the longitudinal one. However, when plotted *versus* their respective r/l_0, the longitudinal and transverse structure functions nearly coincide, raising doubts about an eventual difference between their asymptotic ζ_p exponents (Fig. 9).

This work was supported by DGA/DSP contract No 92/1045, and a SEP contract No 93-0027. We are grateful to O. Metais and J. Jimenez for their numerical data. We are indebted to J.P. Barbier Neyret (I.M.G.) and J.P. Bret (CRTBT) for their technical assistances. We also thank some of the referees for their helpful comments.

Appendix

In a recent work [17], the evolution of δu statistics is seen as a Markovaian process along the scales. The authors first verify the validity of the Chapman-Kolmogorov relation:

$$P(\delta u_3|\delta u_1) = \int P(\delta u_3|\delta u_2)P(\delta u_2|\delta u_1)\mathrm{d}\delta u_2, \qquad (9)$$

where $P(u_1|u_2)$ is the probability density of u_1 for a given u_2. The δu_i:

$$\delta u_i = u\left(x + \frac{r_i}{2}\right) - u\left(x - \frac{r_i}{2}\right),$$

are longitudinal velocity differences at scale r_i ($r_1 > r_2 > r_3$) for the same point x. The authors find good experimental agreement between the two sides of (9). As they remark, this is not a proof, but a good indication for a Markovian behaviour which is also an essential assumption behind (1).

Pushing further, they show that the probability density function of δu is verifying a Fokker-Planck equation where the time is replaced by the logarithm of the scale.

In this appendix, we simply want to signal the connection with what preceeds (which is natural for specialists of random walk).

Limiting ourselves to log-normal G_{rL}, its Laplace transform is:

$$\tilde{G}_{rL}(p) = \int \mathrm{e}^{px} G_{rL}(x)\mathrm{d}x = \exp\left\{ n(r)(C_1 p + C_2 \frac{p^2}{2}) \right\}$$

$$\frac{\partial \tilde{G}_{rL}}{\partial \ln(r)} = (\mathrm{D}C_1 p + \mathrm{D}C_2 \frac{p^2}{2})\tilde{G}_{rL},$$

which is equivalent to the following equation in the direct $(\ln \alpha)$ space:

$$\frac{\partial G_{rL}}{\partial \ln(r)} = \mathrm{D}C_1 \frac{\partial G_{rL}}{\partial \ln \alpha} + \frac{\mathrm{D}C_2}{2} \frac{\partial^2 G_{rL}}{(\partial \ln \alpha)^2} \cdot \qquad (10)$$

Using (1) and the fact that G_{rL} contains all the dependence in the scale:

$$\frac{\partial P_r(\delta u)}{\partial \ln(r)} = \int \frac{\partial G_{rL}}{\partial \ln(r)} (\ln \alpha) \frac{1}{\alpha} P_L(\frac{\delta u}{\alpha}) \mathrm{d} \ln \alpha. \qquad (11)$$

Substituting the expression (10) for $\partial G / \partial \ln(r)$ and integrating in parts gives a Fokker-Planck equation for P_r:

$$\frac{\partial P_r}{\partial \ln(r)} = -\frac{\partial}{\partial \delta u}(\mathrm{D}_1 P_r) + \frac{\partial^2}{(\partial \delta u)^2}(\mathrm{D}_2 P_r),$$

where:

$$\mathrm{D}_1(\delta u) = (\mathrm{D}C_1 + \frac{\mathrm{D}C_2}{2})\delta u; \ \mathrm{D}_2(\delta u) = \frac{\mathrm{D}C_2}{2}\delta u^2.$$

The results of reference [17] are indeed coherent with these dependencies within uncertainties, the main difference being an additional constant in D_2, which could be attributed to a noise.

Note that in equation (9) and in [17] the various δu_i correspond to the same central point x. The knowledge of the correspondence between δu_0 at various scales is fundamental for the direct experimental determination of $\mathrm{D}_1(\delta u)$ and $\mathrm{D}_2(\delta u)$. It would indeed further allow to derive (1) by verifying that the kernel of the relation between P_r and P_L has the assumed form (a convolution in $\ln(\delta u)$). But, as far as we know, this correspondence could be different from the one assumed in [17].

References

1. A. Kolmogorov, Dokl. Akad. Nauk. S.S.S.R. **30**, 301 (1941).
2. A. Kolmogorov, J. Fluid Mech. **13**, 82 (1962).
3. A. Obukhov, J. Fluid Mech. **13**, 77 (1962).
4. G. Parisi, U. Frisch, in *Turbulence and Predictability in Geophysical Fluid Dynamics and Climate Dynamics* (North-Holland, 1985), p. 84.
5. B. Castaing, Y. Gagne, M. Marchand, Physica D **68**, 387 (1993).
6. B. Castaing, Y. Gagne, in *Turbulence in spatially extended systems*, Les Houches, edited by R. Benzi, S. Ciliberto, C. Basdevant (North-Holland, 1993).
7. B. Castaing, B. Dubrulle, J. Phys. II France **5**, 895 (1995).
8. R. Benzi, S. Ciliberto, R. Tripiccione, C. Baudet, F. Massaioli, S. Succi, Phys. Rev. E **48**, R29 (1993).
9. B. Castaing, J. Phys. France **50**, 147 (1989).
10. U. Frisch, M. Vergassola, Europhys. Lett. **14**, 439 (1991).
11. B. Castaing, Y. Gagne, E. Hopfinger, Physica D **46**, 177 (1990).
12. B. Chabaud, A. Naert, J. Peinke, F. Chilla, B. Castaing, B. Hébral, Phys. Rev. Lett. **73**, 3227 (1994).
13. Y. Gagne, M. Marchand, B. Castaing, J. Phys. II France **4**, 1 (1994).
14. B. Castaing, in *Scale invariance and beyond*, edited by B. Dubrulle, F. Graner, D. Sornette (Les Houches, EDP Sciences, Springer, 1997).
15. H. Kahalerras, Y. Malécot, Y. Gagne, B. Castaing, Phys. Fluids **10**, 910 (1998).
16. A. Arnéodo, J. Musy, C. Roux, J. Phys. II France **7**, 363 (1997).
17. R. Friedrich, J. Peinke, Phys. Rev. Lett. **78**, 863 (1997).
18. J. Jiménez, A.W.P. Saffma, R. Rogallo, J. Fluid Mech. **255**, 65 (1993).
19. Y. Saïto, J. Phys. Soc. Jpn **61**, 403 (1992).
20. A. Naert, B. Chabaud, B. Hébral, B. Castaing, in *Advances in Turbulence VI* (Kluwer Academic, 1996), p. 251.
21. R. Benzi, L. Biferal, S. Ciliberto, M.V. Struglia, R. Tripiccione, Physica D **96**, 162 (1996).
22. O. Chanal, Vers les petites échelles dissipatives dans un jet d'hélium gazeux à basse température. PhD thesis, Institut National Polytechnique de Grenoble, 1998.
23. V. Emsellem, P. Kadanoff, D. Lohse, P. Tabeling, J. Wang, Phys. Rev. E **55**, 2672–2684 (1997).
24. F. Anselmet, Y. Gagne, E. Hopfinger, R. Antonia, J. Fluid Mech. **140**, 63 (1984).
25. M. Marchand, Propriétés statistiques des petites structures dans les écoulements turbulents : Influence du nombre de reynolds sur l'intermittence. PhD thesis, Institut National Polytechnique de Grenoble, 1994.
26. Y. Malécot, Intermittence en turbulence 3D : statistiques de la vitesse et de la vorticité. PhD thesis, Université de Grenoble, 1998.
27. J. Jiménez, A. Wray, in *Center for Turbulence Research* (Stanford University, 1994), p. 287.
28. A. Arnéodo, S. Manneville, J. Musy, Eur. Phys. J. B **1**, 129 (1998).
29. A. Arnéodo, C. Baudet, F. Belin, R. Benzi, B. Castaing, B. Chabaud, R. Chavarria, S. Ciliberto, R. Camussi, F. Chillà, B. Dubrulle, Y. Gagne, B. Hébral, J. Herweijer, M. Marchand, J. Maurer, W. van de Water, H. Willaime, Europhys. Lett. **36**, 411 (1996).
30. S. Chen, K. Sreenivasan, M. Nelkin, N. Cao, Phys. Rev. Lett. **79**, 2253 (1997).
31. J. Herweijer, W. van de Water, in *Advances in Turbulence V* (Kluwer Academic, 1995), p. 210.
32. V. L'vov, E. Podivilov, I. Procaccia, Phys. Rev. Lett. **79**, 2050 (1997).
33. M. Lesieur, O. Métais, Annu. Rev. Fluid. Mech. **28**, 45–82 (1996).
34. O. Métais, M. Lesieur, in *Advances in Turbulence II* (Springer, 1989), pp. 371–376.
35. J. Smagorinsky, Mon. Weath. Rev. **91**, 99–164 (1963).